

A&A manuscript no. (will be inserted by hand later)
Your thesaurus codes are: 06

A multifrequency analysis of radio variability of blazars

A. Ciaramella^{1,7}, C. Bongardo², H.D. Aller³, M.F. Aller³, G. De Zotti², A. Lähteenmaki⁴, G. Longo^{5,6},
L. Milano^{5,6}, R. Tagliaferri^{1,7}, H. Teräsranta⁴, M. Tornikoski⁴, and S. Urpo⁴

¹ Dipartimento di Matematica ed Informatica, Università di Salerno, via S. Allende, Baronissi (Sa), Italy

² INAF–Osservatorio Astronomico di Padova, Vicolo dell’Osservatorio 5, I-35122 Padova, Italy

³ Dept. of Astronomy, Dennison Bldg., U. Michigan, Ann Arbor, MI 48109, USA

⁴ Metsähovi Radio Observatory, 02540 Kylmälä, Finland

⁵ Dipartimento di Scienze Fisiche, Università Federico II, via Cinthia 6, I-80126 Napoli, Italy

⁶ INFN - Sezione di Napoli, via Cinthia 6, I-80126 Napoli, Italy

⁷ INFN - Sezione di Salerno, via S. Allende, Baronissi (SA), Italy

Received ; accepted

Abstract. We have carried out a multifrequency analysis of the radio variability of blazars, exploiting the data obtained during the extensive monitoring programs carried out at the University of Michigan Radio Astronomy Observatory (UMRAO, at 4.8, 8, and 14.5 GHz) and at the Metsähovi Radio Observatory (22 and 37 GHz). Two different techniques detect, in the Metsähovi light curves, evidences of periodicity at both frequencies for 5 sources (0224 + 671, 0945 + 408, 1226 + 023, 2200 + 420, and 2251 + 158). For the last three sources consistent periods are found also at the three UMRAO frequencies and the Scargle (1982) method yields an extremely low false-alarm probability. On the other hand, the 22 and 37 GHz periodicities of 0224 + 671 and 0945 + 408 (which were less extensively monitored at Metsähovi and for which we get a significant false-alarm probability) are not confirmed by the UMRAO database, where some indications of ill-defined periods about a factor of two longer are retrieved. We have also investigated the variability index, the structure function, and the distribution of intensity variations of the most extensively monitored sources. We find a statistically significant difference in the distribution of the variability index for BL Lac objects compared to flat-spectrum radio quasars (FSRQs), in the sense that the former objects are more variable. For both populations the variability index steadily increases with increasing frequency. The distribution of intensity variations also broadens with increasing frequency, and approaches a log-normal shape at the highest frequencies. We find that variability enhances by 20–30% the high frequency counts of extragalactic radio-sources at bright flux densities, such as

those of the WMAP and PLANCK surveys. In all objects with detected periodicity we find evidence for the existence of impulsive signals superimposed on the periodic component.

Key words: Methods: data analysis – BL Lacertae objects: general – quasars: general – radio continuum: general

1. Introduction

The name Blazars identifies a family of radio-loud Active Galactic Nuclei (AGNs) showing a rather complex phenomenology: extreme variability at all wavelengths, polarization, strong γ -ray emission, brightness temperatures exceeding the Compton limit (Urry 1999). The large amount of work done in the last decade has led to a rather general consensus on the global mechanism responsible for the emission: a rotating black hole surrounded by a massive accretion disk with an intense plasma jet closely aligned to the line of sight. Relativistic electrons produce the soft photons through synchrotron emission, while hard photons are produced by inverse Compton scattering. This overall scenario, however, still presents a large number of poorly understood details which, in turn, lead to a wide variety of models and call for long term and multi-wavelength campaigns capable to provide the necessary observational constraints.

Variability measurements provide key information on the AGN structure, down to linear scales or flux density levels not accessible with interferometric imaging. The most extensive blazar monitoring campaigns have been carried out at radio frequencies. The University of Michi-

Send offprint requests to: A. Ciaramella: ciaram@unisa.it

gan monitoring program at 4.8, 8.0 and 14.5 GHz has obtained data on over 200 sources for over three decades. At higher frequencies, the Metsähovi group (Teräsraanta et al. 1998) have reported observations at 22, 37 and 87 GHz of 157 extragalactic radio sources, many of which have been monitored for over 20 years. The Bologna group (Bondi et al. 1996) have observed at 408 MHz 125 radio sources for 15 years. A multifrequency monitoring of large sample of compact radio sources has been carried out by Kovalev et al. (2002) with the RATAN-600 telescope.

The mechanisms for variability are still not well understood. Possibilities discussed in the literature include shocks in jets (Marscher & Gear 1985; Aller, Aller & Hughes 1985; Marscher 1996) and changes in the direction of forward beaming [due, e.g. to helical trajectories of plasma elements (Camenzind & Krockenberger 1992) or to a precessing binary black-hole system (Begelman et al. 1980; Sillanpää et al. 1988)], introducing flares due to the lighthouse effect. Thus, variability furnishes important clues into size, structure, physics and dynamics of the radiating source region.

The cm-wavelength variability of extragalactic sources has been investigated by Hughes et al. (1992) and Aller et al. (1996, 2003) exploiting the uniquely large, long term, University of Michigan Radio Astronomy Observatory (UMRAO) data-base. Kelly et al. (2003) applied a cross-wavelet transform to analyze the UMRAO light curves of the Pearson-Readhead VLBI survey sources. The Metsähovi data-base has been analyzed by Lainela & Valtaoja (1993), Teräsraanta & Valtaoja (1994), Valtaoja et al. (1999), Lähteenmäki et al. (1999), Lähteenmäki & Valtaoja (1999).

Still, the information content of the radio-monitoring data-base has not yet been fully exploited. We are interested, in particular, in utilizing it to predict the effect of radio-source variability on the high-frequency all-sky surveys to be carried out by ESA's PLANCK mission. Such predictions are useful to plan the quick-look analysis of PLANCK data and to organize follow-up observations. To this end, the Metsähovi data, taken at frequencies close to those of PLANCK-LFI (Low Frequency Instrument) channels, are particularly well fit.

Another very interesting, highly debated issue, is the possible presence of periodicities in the blazar light curves. Claims for the existence of periodic behavior are mostly based on optical data (Lainela et al. 1999; Fan 2000, Fan et al. 2002, and references therein). The most famous, but still somewhat controversial, case is the 11.65 year periodicity of OJ287 (Sillanpää et al. 1988, 1996; Marchenko et al. 1996; Hagen-Thorn et al. 1997; Pietilä et al. 1999). Evidence of a persistent modulation of the radio total flux and polarization of this source, with period of ~ 1.66 yr was found by Aller et al. (1992) and Hughes et al. (1998).

A possible periodicity of ~ 5.7 years in the radio light-curve of the BL Lac object AO 0235+16 has been reported by Roy et al. (2000) and Raiteri et al. (2001). Indications

of a periodic or quasi-periodic component with a time-scale of 5.5–6 years (close to that of AO 0235 + 16) of the radio emission of the BL Lac object S5 0716 + 714 were found by Raiteri et al. (2003)

In this paper we present a new investigation of radio light curves of a sample of blazars, exploiting more effective techniques than the Periodogram method commonly used (in various versions) for periodicity analysis. The maximum time interval covered by the data we used is 1979–2001 in the case of Metsähovi, 1965–1999 in the case of UMRAO. The techniques used are described in Section 2 and the main results are presented in Section 3. In Section 4 we discuss the multifrequency variability properties for a blazar sample monitored by both the UMRAO and the Metsähovi Radio Observatory, and estimate the effect of variability on high-frequency counts of such objects. In Section 5 we summarize our main conclusions.

2. The time series analysis

In what follows, we shall assume x to be a physical variable measured at discrete times t_i ; $x(t_i)$ can be written as the sum of the signal x_s and random errors R :

$$x_i = x(t_i) = x_s(t_i) + R(t_i) . \quad (1)$$

The problem is how to estimate possible fundamental frequencies which may be present in the signal $x_s(t_i)$. In the case of even sampling, many Fourier-like tools can be effectively used (cf. Fernie 1979; Horne & Baliunas 1986). These methods, however, encounter problems when dealing with unevenly sampled data and shortcuts like the use of interpolation to re-sample the data, introduce a noise amplification which usually undermines the subsequent use of Fourier based techniques which are notoriously very sensitive to the noise level of the input data (cf. Kay 1988; Marple 1987, but see also Horowitz 1974).

2.1. The Periodogram (P) method

The most commonly used tool for periodicity analysis of both evenly and unevenly sampled signals is the so called Periodogram (hereafter P), which is an estimator of the signal energy in the frequency domain (Deeming 1975), and has been extensively applied to the study of light curves of variable stars, both periodic and semi-periodic.

In the case of even sampling, the Periodogram has a simple statistic distribution (exponentially distributed for Gaussian noise). This, however, is no longer true for unevenly sampled data, thus making it difficult to control errors (Kay 1988; Marple 1987; Oppenheim & Shafner 1965). Scargle (1982) and Lomb (1976) introduced a modified form of Periodogram which takes explicitly into account the effects of uneven sampling.

Let f be the frequency and τ a shift variable, and let us also suppose that we are dealing with an observation

Table 1. Objects for which we have positive detection of periodicity on Metsähovi daily averaged data. Column 1: object identification. Columns 2-5: 22 GHz data; columns 6-9: 37 GHz data. Columns 2 & 6: number of data points; columns 3 & 7: maximum admissible period to avoid aliasing; columns 4 & 8: period (in units of 10^3 days) obtained by STIMA; column 5 & 9: period obtained from the Lomb's Periodogram.

Name	N	Mx. P. ($\times 10^3$)	STIMA ($\times 10^3$)	Lomb ($\times 10^3$)	N	Mx. P. ($\times 10^3$)	STIMA ($\times 10^3$)	Lomb ($\times 10^3$)	Notes
(1)	(2)	(3)	(4)	(5)	(6)	(7)	(8)	(9)	(10)
0224 + 671	76	3.062	1.021	1.021	63	3.668	0.950	0.970	few points
0945 + 408	47	3.742	1.386	1.336	26	4.467	1.313	1.240	
1226 + 023	694	6.665	3.029	2.777	716	7.822	3.260	1.261	
2200 + 420	644	6.676	3.034	3.034	715	7.873	2.811	3.028	
2251 + 158	571	6.676	2.384	2.384	549	7.538	2.217	2.512	

Table 2. Analysis of UMRAO data on Metsähovi sources with detected periodicity (Table 1). Columns 2-5, 6-9, and 10-13 refer to 4.8, 8.0, and 14.5 GHz data, respectively.

Name	N	Mx. P. ($\times 10^3$)	STIMA ($\times 10^3$)	Lomb ($\times 10^3$)	N	Mx. P. ($\times 10^3$)	STIMA ($\times 10^3$)	Lomb ($\times 10^3$)	N	Mx. P. ($\times 10^3$)	STIMA ($\times 10^3$)	Lomb ($\times 10^3$)
(1)	(2)	(3)	(4)	(5)	(6)	(7)	(8)	(9)	(10)	(11)	(12)	(13)
0224 + 671	110	5.998	1.764	1.764	119	6.859	2.286	2.286	110	7.592	2.109	2.109
0945 + 408	73	6.048	–	–	126	7.993	–	–	92	5.920	2.690	2.466
1226 + 023	493	6.424	3.197	3.197	1294	1.232	3.082	3.082	760	9.114	3.038	3.038
2200 + 420	745	7.844	2.801	2.801	1212	1.131	2.261	1.413	1056	9.056	2.830	2.830
2251 + 158	554	7.674	2.240	2.240	1175	1.195	2.390	2.490	885	9.190	2.297	2.297

Table 3. Summary of detected periods (in units of 10^3 days).

Name	4.8 GHz	8.0 GHz	14.5 GHz	22 GHz	37 GHz
0224+671	1.764	2.286	2.109	1.021	0.950
0945+408	–	–	2.690	1.386	1.313
1226+023	3.197	3.082	3.038	3.029	3.260
2200+420	2.801	2.261	2.830	3.034	2.811
2251+158	2.240	2.390	2.297	2.384	2.217

series formed by N points $x(n)$. Their mean and variance are given by:

$$\bar{x} = \frac{1}{N} \sum_{n=1}^N x(n) \quad \text{and} \quad \sigma^2 = \frac{1}{N-1} \sum_{n=1}^N (x(n) - \bar{x})^2. \quad (2)$$

The normalized Lomb's P^L , i.e. the power spectrum as a function of the angular frequency $\omega \equiv 2\pi f > 0$ is defined as:

$$P_N^L(\omega) = \frac{1}{2\sigma^2} \left[\frac{\left[\sum_{n=0}^{N-1} (x(n) - \bar{x}) \cos \omega(t_n - \tau) \right]^2}{\sum_{n=0}^{N-1} \cos^2 \omega(t_n - \tau)} \right] + \frac{1}{2\sigma^2} \left[\frac{\left[\sum_{n=0}^{N-1} (x(n) - \bar{x}) \sin \omega(t_n - \tau) \right]^2}{\sum_{n=0}^{N-1} \sin^2 \omega(t_n - \tau)} \right] \quad (3)$$

and τ is defined by the equation:

$$\tan(2\omega\tau) = \frac{\sum_{n=0}^{N-1} \sin 2\omega t_n}{\sum_{n=0}^{N-1} \cos 2\omega t_n}. \quad (4)$$

2.2. Autocorrelation matrix based analysis: the STIMA approach

Recently, more effective techniques based on the analysis of the signal autocorrelation matrix were introduced [for a detailed exposition of the problem see Kay (1988) and Marple (1987)]. In a previous paper (Tagliaferri et al. 1999, hereafter T99) some of us introduced the so called STIMA algorithm, based on a particular type of the MULty Signal Classifier (MUSIC) (Oppenheim & Schaffer 1965) estimator specifically tailored to work with unevenly sampled data and on a robust nonlinear PCA Neural Network used to extract the principal components of the autocorrelation matrix of the input sources. Without entering into details (which may be found in T99) we now briefly summarize its main features.

Let us assume to have a signal with p sinusoidal components (narrow band). The p sinusoids are modelled as a stationary ergodic signal, and this is possible only if the phases are assumed to be independent random variables uniformly distributed in the interval $[0, 2\pi]$. To estimate the frequencies of these components we exploit the prop-

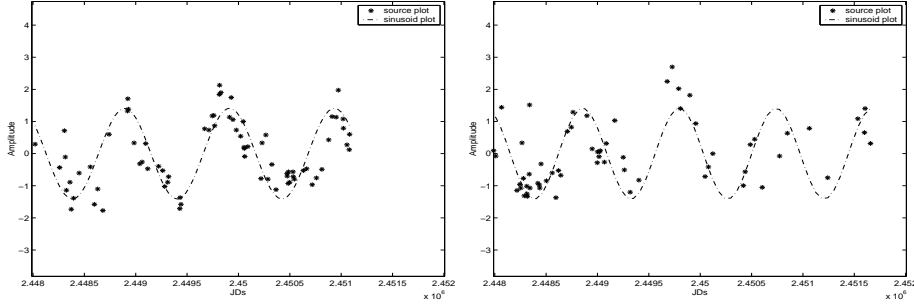


Fig. 1. A0224+671. Results for the 22 GHz (left panel) and 37 (right panel), daily averaged datasets. Sinusoids with a period equal to those provided by STIMA and listed in Tables 1 and 2 are overplotted as a visual aid to recognize periodicities. It needs to be stressed that these curves must be regarded as visual aids only: their amplitude is not by any means related to the signal.

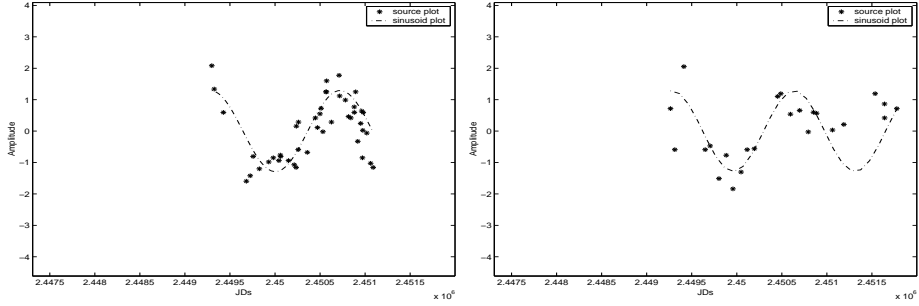


Fig. 2. 0945 + 408. Results for the 22 (left) and 37 GHz (right) M dataset. Sinusoids as in Fig. 1

erties of the signal autocorrelation matrix (a.m.) which is the sum of the signal and the noise matrices. The p principal eigenvectors of the signal matrix allow the estimate of frequencies; the p principal eigenvectors of the signal matrix are the same of the total matrix. In order to extract the principal components we use a robust nonlinear PCA Neural Network and we apply a modified version of MUSIC that can be applied directly on unevenly sampled data, to obtain the periodicities (cf. T99 and references therein).

The STIMA process for periodicity analysis can be divided in the following steps:

- **Preprocessing:** we first calculate and subtract the average pattern to obtain a zero mean process (Karhunen & Joutsensalo 1994, 1995).
- **Neural computing:** the fundamental learning parameters are: i) the initial weight matrix; ii) the number of neurons, which is the number of principal eigenvectors that we need, and therefore is equal to twice the number of signal periodicities (for real signals); iii) α , the nonlinear learning function parameter; iv) the learning rate μ .

We then initialize the weight matrix \mathbf{W} assigning the classical small random values. Otherwise we can use the first patterns of the signal as the columns of the matrix.

Experimental results show, however, that even though the latter technique speeds up the convergence of our neural estimator (*n.e.*), it cannot be used with anomalously shaped signals, such as stratigraphic geological signals. We use a simple criterion to decide whether the neural network has reached or not convergence: we control when the Power Spectrum of a modified MUSIC estimator is greater than zero. This modified MUSIC estimator can be written as:

$$P_M = \frac{1}{M - \sum_{i=1}^M |\mathbf{e}_f^H \mathbf{w}(i)|^2} \quad (5)$$

where $\mathbf{w}(i)$ is the i -th weight vector after learning, and \mathbf{e}_f^H is the sinusoidal vector:

$$\mathbf{e}_f^H = [e_f^{t_0}, e_f^{t_1}, \dots, e_f^{t_{L-1}}]^H \quad (6)$$

and t_0, \dots, t_{L-1} , are the epochs of the first L samplings.

We then have the following general algorithm:

- **STEP 1:** initialize the weight vectors $\mathbf{w}_0(i) \forall i = 1, \dots, p$ with small random values, or with orthonormalized signal patterns. Then initialize the learning threshold ϵ and the learning rate μ . Then reset pattern counter $k = 0$.
- **STEP 2:** input the k -th pattern

$$\mathbf{x}_k = [x(k), \dots, x(k + N + 1)]$$

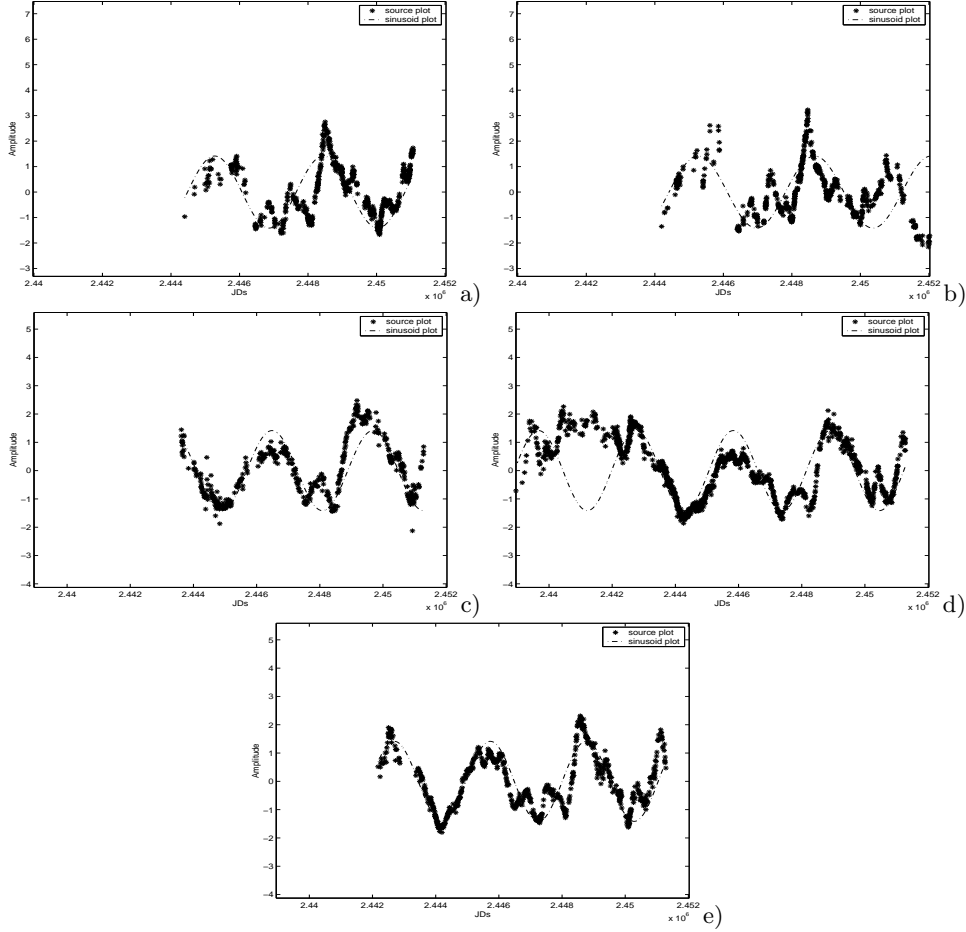


Fig. 3. 1226+023. Panels a and b: results for the 22 GHz and the 37 GHz daily averaged radio curves, respectively. Panels c, d and e: the same for the 4.8, 8 and 14.5 GHz data, respectively. Sinusoids with a period equal to those listed in the tables are overplotted as visual aid (as in Fig.1).

where N is the number of input components.

- STEP 3: calculate the output for each neuron $y(j) = \mathbf{w}^T(j)\mathbf{x}_i, \forall i = 1, \dots, p$.

- STEP 4: $\forall i = 1, \dots, p$ modify the weights

$$\mathbf{w}_{k+1}(i) = \mathbf{w}_k(i) + \mu_k g(y_k(i)) \mathbf{e}_k(i)$$

- STEP 5: convergence test. If

$$P_M \frac{1}{M - \sum_{i=1}^M |\mathbf{e}_f^H \mathbf{w}(i)|^2} > 0$$

, then GO TO STEP 7.

- STEP 6: $k = k + 1$. GO TO STEP 2.

- STEP 7. End.

The frequency estimator MUSIC takes as input the weight matrix columns after the learning phase. The estimated signal frequencies are obtained as the peak locations of the function previously introduced. When f is the frequency of the i -th sinusoidal component, $f = f_i$, we have $P_M \rightarrow \infty$. In practice, we have a peak near and

in correspondence to the component frequency. Estimates are therefore related to the highest peaks.

We note that MUSIC works on individual points, not on the basis of time intervals; it therefore does not need any kind of interpolation to deal with gaps in the data. Also, tests carried out by the Authors of this method (Tagliaferri et al. 1999) have shown that low-frequency drifts of the baseline flux of sources do not affect the derived periodicities.

In the following discussion we shall make use of both STIMA and the Lomb Periodogram.

3. Analysis of the Metsähovi radio light curves

We have analyzed the 22 and 37 GHz, both daily and weekly averaged, light curves of blazars monitored with the Metsähovi radio telescope, updated to the end of 2001.

In order to establish whether a periodicity is real or not we adopted the following set of rules:

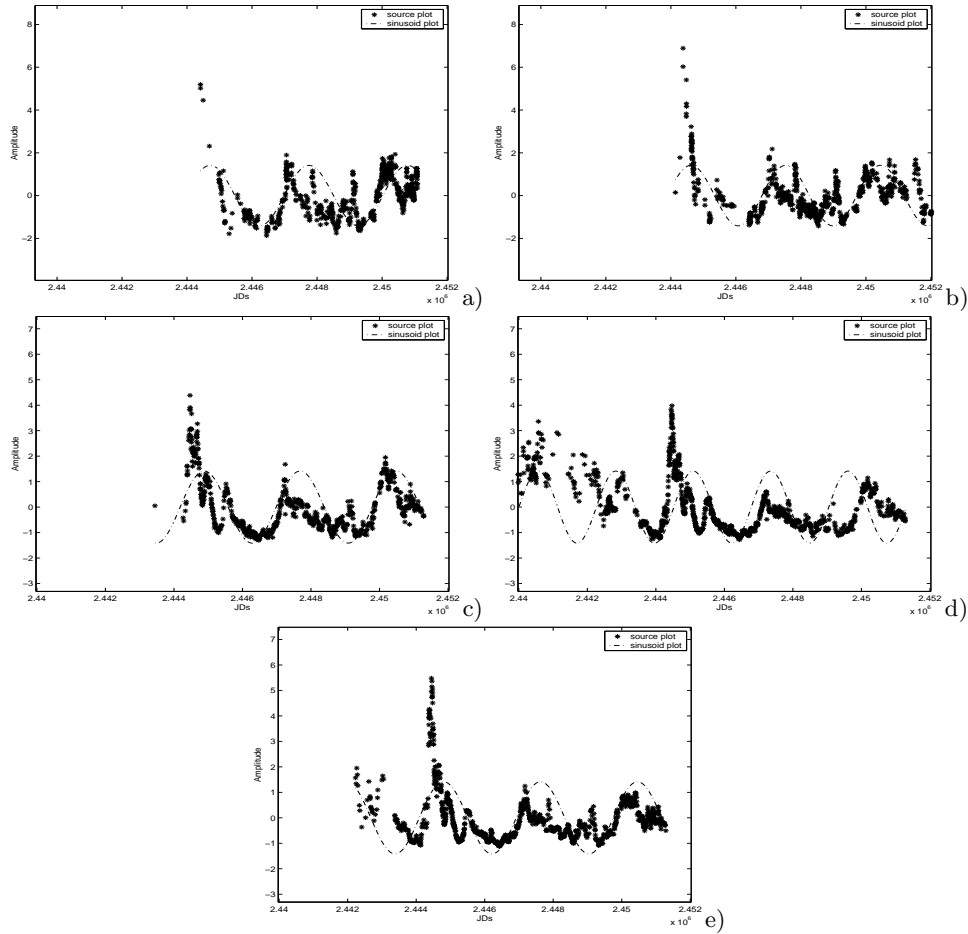


Fig. 4. 2200 + 420. Panels have the same meaning as in Fig. 3.

- the periodicity derived by both STIMA and Lomb’s method must be shorter than 1/2 of the time coverage (in order to avoid aliasing);
- For a given object, periodicity must be found in both the 22 and the 37 light curves and the periods must be equal given a percentage of error (in the following we use a percentage of 10%)

Of the 157 sources in the sample by Teräsranta et al. (1998), 80 could not be analyzed due to either a very short time coverage or a too sparse distribution of the data points. Evidence of a periodicity was found for 5 of the remaining 77 objects (see Figs. 1–5). The results for these, based on daily averaged fluxes, are given in Table 1, where the left-hand side refers to 22 GHz data, the right-hand side to 37 GHz. The periodicity, given in units of 10^3 days, is detected by both STIMA and Lomb’s methods and both methods yield, for each source, values very close to each other; the maximum difference is of $\simeq 8\%$. In the following, unless explicitly noted, we shall always use the STIMA estimate, which is less affected by spurious signals. If weekly, rather than daily, estimates are used, to increase the S/N ratio, the estimated periods are

essentially unaffected (differences are at percent levels), even though the significance of periodicity is somewhat increased.

Table 2 summarizes the results of the analysis of the UMRAO monitoring data for the five sources with detected periodicity, while a compendium of STIMA periods at the five UMRAO plus Metsähovi frequencies is presented in Table 3.

For the sources 0224 + 671 (Fig. 1) and 0945 + 408 (Fig. 2) the number of data points is quite limited and, correspondingly, the periods are ill-defined. In the case of A0224 + 671 the analysis of UMRAO data yields significantly different periods at 4.8 GHz compared to 8 and 14.5 GHz; all of them are substantially higher (by roughly a factor of 2) than those found from the Metsähovi light curves. For 0945 + 408 (Fig. 2) no periodicity was found at 4.8 and 8.0 GHz, while an ill-defined period of 2690 days (STIMA), about a factor of 2 larger than found at the Metsähovi frequencies, could be present in the 14.5 GHz signal. These sources are good candidates for longer and more frequently sampled monitoring campaigns, particularly at the Metsähovi frequencies where the time span of light curves is relatively short.

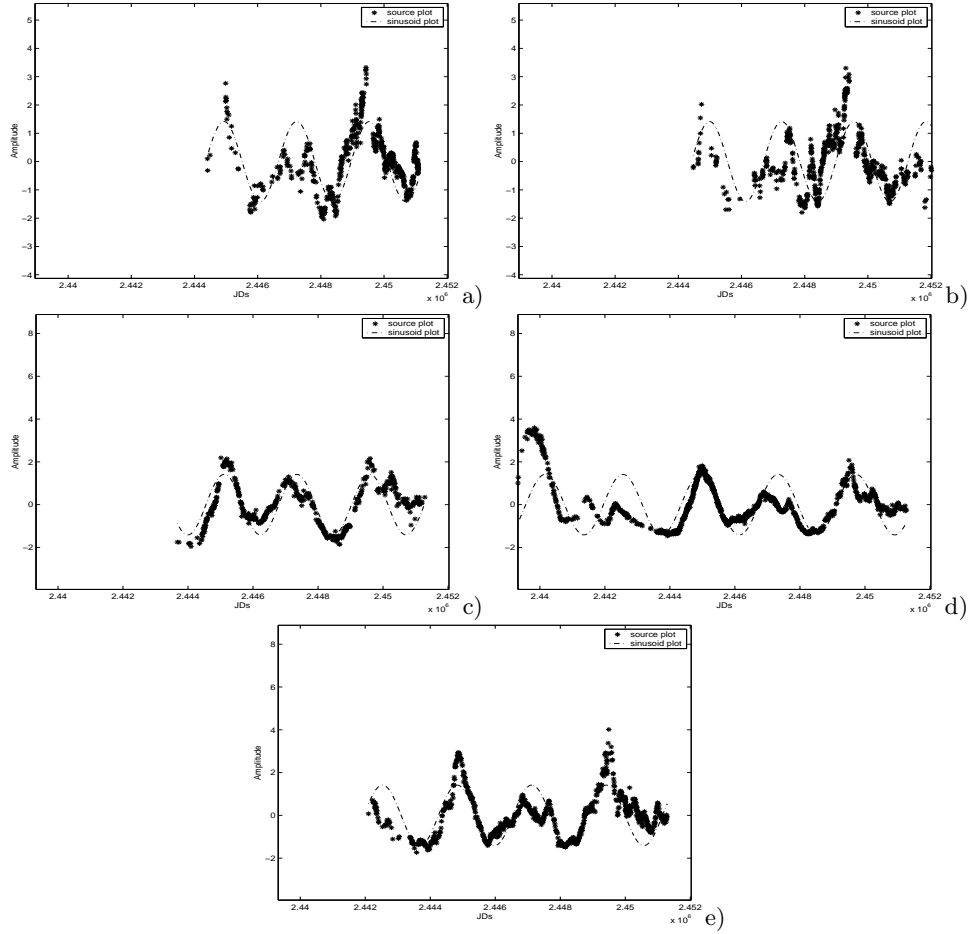


Fig. 5. 2251 + 158. Panels have the same meaning as in Fig. 3.

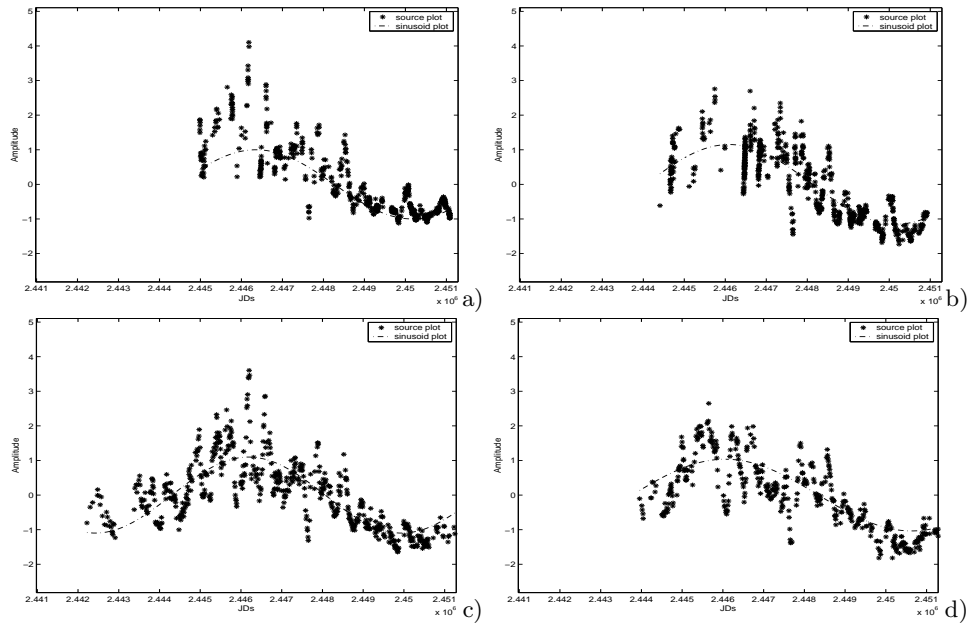


Fig. 6. OJ287. Panels a), b), c), and d): light curves at 22, 37, 14.5, and 4.8 GHz, respectively. The dot-dashed sinusoids have periods of about 20.9 yr (22 GHz), 22.3 yr (37 GHz), 20.6 yr (14.5 GHz), 25 yr (4.8 GHz).

Table 4. The U sample with source classifications by Donato et al. (2001) and Teräsraanta et al. (1998). In the latter case BLO stands for BL Lac Object. Redshifts were taken from the SIMBAD astronomical database.

Name	Other name	Donato	Teräsraanta	z
0048-097	OB -080	LBL	BLO	0.2
0133+476 [†]	OC 457	FSRQ	HPQ	0.859
0202+149 [†]	4C 15.05	FSRQ	HPQ	0.405
0235+164 [†]	OD 160	LBL	BLO	0.94
0420-014 [†]	OF -135	FSRQ	HPQ	0.915
0430+052 [†]	3C 120	FSRQ	LPQ*	0.0331
0605-085	OH -010		HPQ	0.872
0607-157 [‡]	OH 112			0.324
0735+178 [†]	OI 158	LBL	BLO	0.424
0814+425 [†]	OJ 425	LBL	BLO	0.2453
0851+202 [†]	OJ 287	LBL	BLO	0.306
0923+392 [†]	4C 39.25	FSRQ	LPQ	0.6948
0945+408	4C 40.24	FSRQ	LPQ	1.252
0954+658		LBL	BLO	0.367
1034-293	OL -259	FSRQ	HPQ*	0.312
1055+018 [†]	OL 093	FSRQ	HPQ	0.888
1127-145 [‡]	OM -146			1.187
1226+023 [†]	3C 273	FSRQ	LPQ	0.158
1253-055 [†]	3C 279	FSRQ	HPQ	0.538
1308+326 [†]	OP 313	LBL	BLO	0.996
1418+546 [†]	OQ 530	LBL	BLO	0.151
1510-089 [†]	OR -017	FSRQ	HPQ	0.359
1538+149	OR 165	LBL	BLO	0.605
1637+574 [†]	OS 562		LPQ	0.7506
1641+399 [†]	3C345	FSRQ	HPQ	0.594
1642+690	4C 69.21		HPQ	0.751
1749+096 [†]	OT 081	LBL	BLO	0.322
1749+701		LBL	BLO	0.77
1823+568	4C 56.27	LBL	BLO	0.6635
1928+738	4C 73.18	FSRQ	LPQ	0.360
2131-021	4C -02.18	LBL	BLO	1.285
2134+004 [†]	OX 057	FSRQ	LPQ	1.931997
2145+067 [†]	OX 076		LPQ	0.99
2155-152 [‡]	OX -192	FSRQ		0.672
2200+420 [†]	BL Lac	LBL	BLO	0.0688
2201+315 [†]	4C 31.63		LPQ	0.298
2223-052 [†]	3C 446	FSRQ	HPQ	1.404
2251+158 [†]	3C 454.3	FSRQ	HPQ	0.859
2254+074 [†]	OY 091	LBL	BLO	0.19

[†] Also in the Metsähovi database.

[‡] Classified as FSRQ by Stickel et al. (1994).

* Classified by Ghisellini et al. (1993).

In the case of 1226 + 023 (Fig. 3), the analysis of the UMRAO database yields well defined periods at all frequencies (4.8, 8, and 14.5 GHz). The periodic behavior is most evident at 4.8 and 8 GHz, but the estimated period at 8 GHz is lower by $\sim 20\%$ than at 4.8 GHz. At higher frequencies (14.5, 22 and 37 GHz) the periodic signal appears to be contaminated by an additional impulsive component which becomes dominant at 14.5 GHz. The estimated pe-

riods at all frequencies, except 8 GHz, are consistent with each other to better than 10%.

Periodicity is detected, by both the STIMA and the Lomb's methods, in light curves of 2200 + 420 at all frequencies (Fig. 4), and period estimates are all consistent with each other, and close to the value obtained in the optical: 7.8 ± 0.2 yr, i.e. 2849 ± 73 days (Marchenko et al. 1996; Hagen-Thorn et al. 1997). The periodicity is again most evident at 4.8 and 8 GHz, while at 22 and 37 GHz the residuals show the presence of an additional impulsive signal. At 14.5 GHz, the evidence of periodicity is marginal, although the estimated period is very close to that found in the other bands.

As shown by Fig. 5, 2251 + 158 is probably our best case. Strong and consistent periodic signals are detected at all frequencies, most clearly at 22, 4.8 and 8.0 GHz. At all frequencies, however, an inspection of the the residuals obtained by subtracting the first harmonic from the observed data, evidences an additional, impulsive, source of luminosity variations, over-imposed on the underlying periodic component.

It may look surprising that our list of sources with evidence for periodicity does not include the most famous case, OJ287. The reason is that the estimated period does not meet our criterion of being shorter than 1/2 of the time coverage. In fact, we detect a possible modulation on a period of about 21–22 years at 14.5, 22, and 37 GHz, and on a longer period (about 25 years) at 4.8 GHz (see Fig. 6). These possible periodicities are about a factor of 2 larger than found by analyses of optical data (Sillanpää et al. 1988, 1996; Pietilä et al. 1999). An analysis of the residuals (after having subtracted the sinusoidal modulation) detects a significant periodicity of ~ 1.6 yr at 22, 37, and 14.5, in close agreement with that found by Aller et al. (1992) using a Scargle periodogram and by Hughes et al. (1998) using a wavelet transform. Data at 8 and 4.8 GHz indicate (in the residuals) somewhat longer periods (1.7 and 2.05 yr, respectively).

4. Phenomenology of variability properties

The use of unbiased samples is essential for meaningful statistical analyses. The UMRAO group have monitored and analyzed the light curves of two complete samples, the Pearson-Readhead sample (Aller et al. 2003) and a BL Lac sample (Aller et al. 1999).

The sample used in the present analysis is drawn from the complete catalog of sources brighter than 1 Jy at 5 GHz (Kühr et al. 1981). We have have selected the Kühr sources with UMRAO monitoring at 8 GHz for a total of ≥ 3000 days, with gaps not exceeding 200 days, all times being computed *in the source frame* ($t_{\text{source}} = t_{\text{observer}}/(1+z)$). Also, we have confined ourselves to sources classified either as Low-energy peak BL Lacs (LBLs, Padovani & Giommi 1995) or Flat-Spectrum Radio Quasars (FSRQ), thus excluding the lonely High-

Table 5. Mean values of the variability index.

Type	N	37 GHz	22 GHz	14.5 GHz	8 GHz	4.8 GHz
LBL	9	0.74±0.27	0.73±0.26	0.69±0.19	0.68±0.18	0.59±0.16
FSRQ	16	0.61±0.16	0.55±0.15	0.54±0.12	0.50±0.11	0.38±0.08
HPQ	9	0.65±0.23	0.60±0.22	0.56±0.17	0.51±0.16	0.38±0.12
LPQ	7	0.56±0.23	0.48±0.21	0.49±0.18	0.45±0.17	0.33±0.13

Table 6. KS test on the distributions of variability indices.

	37 GHz		22 GHz		14.5 GHz		8 GHz		4.8 GHz	
	d	prob	d	prob	d	prob	d	prob	d	prob
LBL vs FSRQ	0.65	7.3 10 ⁻³	0.67	5.7 10 ⁻³	0.52	7.2 10 ⁻³	0.61	1.4 10 ⁻²	0.67	1.8 10 ⁻⁴
HPQ vs LPQ	0.32	0.73	0.46	0.28	0.39	0.33	0.32	0.73	0.28	0.75

Table 7. Mean values of structure function slopes.

Type	37 GHz	22 GHz	14.5 GHz	8 GHz	4.8 GHz
all	1.14 ± 0.23	1.18 ± 0.25	1.17 ± 0.19	1.17 ± 0.20	1.21 ± 0.20
LBL	0.98±0.37	0.95±0.37	1.05±0.29	1.00±0.28	1.05±0.29
FSRQ	1.08±0.29	1.16±0.31	1.15±0.25	1.19±0.26	1.23±0.27
HPQ	1.05±0.40	1.09±0.41	1.08±0.35	1.18±0.38	1.14±0.37
LPQ	0.96±0.43	1.07±0.48	1.15±0.44	1.17±0.46	1.24±0.47

energy peak BL Lac (HBL), namely Mkn 501, as well as the few sources classified as radio-galaxies or Seyfert galaxies. Whenever available, we have adopted the classification given by Donato et al. (2001), supplemented with those by Teräsranta et al. (1998), Ghisellini et al. (1993), and by Stickel et al. (1994).

The final sample comprises 39 sources (24 FSRQs and 15 LBLs), listed in Table 4 (U sample). Of these sources, 25 (9 LBLs and 16 FSRQs) were also extensively monitored by the Metsähovi group (U∩M sample). Of the 24 FSRQs, 21 are classified as either HPQ (12) or LPQ (9); the acronyms stand for high- or low-polarization quasars, respectively. Redshift determinations are available for all sources. To characterize the variability properties at the various frequencies we have computed the variability index (V.I.), the structure function (Simonetti et al. 1985; Hughes et al. 1992), and the distribution of intensity variations. The variability index has been computed allowing for measurement errors following Aller et al. (2003):

$$V.I. = \frac{(S_{max} - \sigma_{S_{max}}) - (S_{min} + \sigma_{S_{min}})}{(S_{max} - \sigma_{S_{max}}) + (S_{min} + \sigma_{S_{min}})}. \quad (7)$$

Again following Aller et al. (2003) we have excluded anomalously noisy data, i.e. data with $\sigma_S > \max(0.1 \text{ Jy}, 0.03S)$.

4.1. Variability index

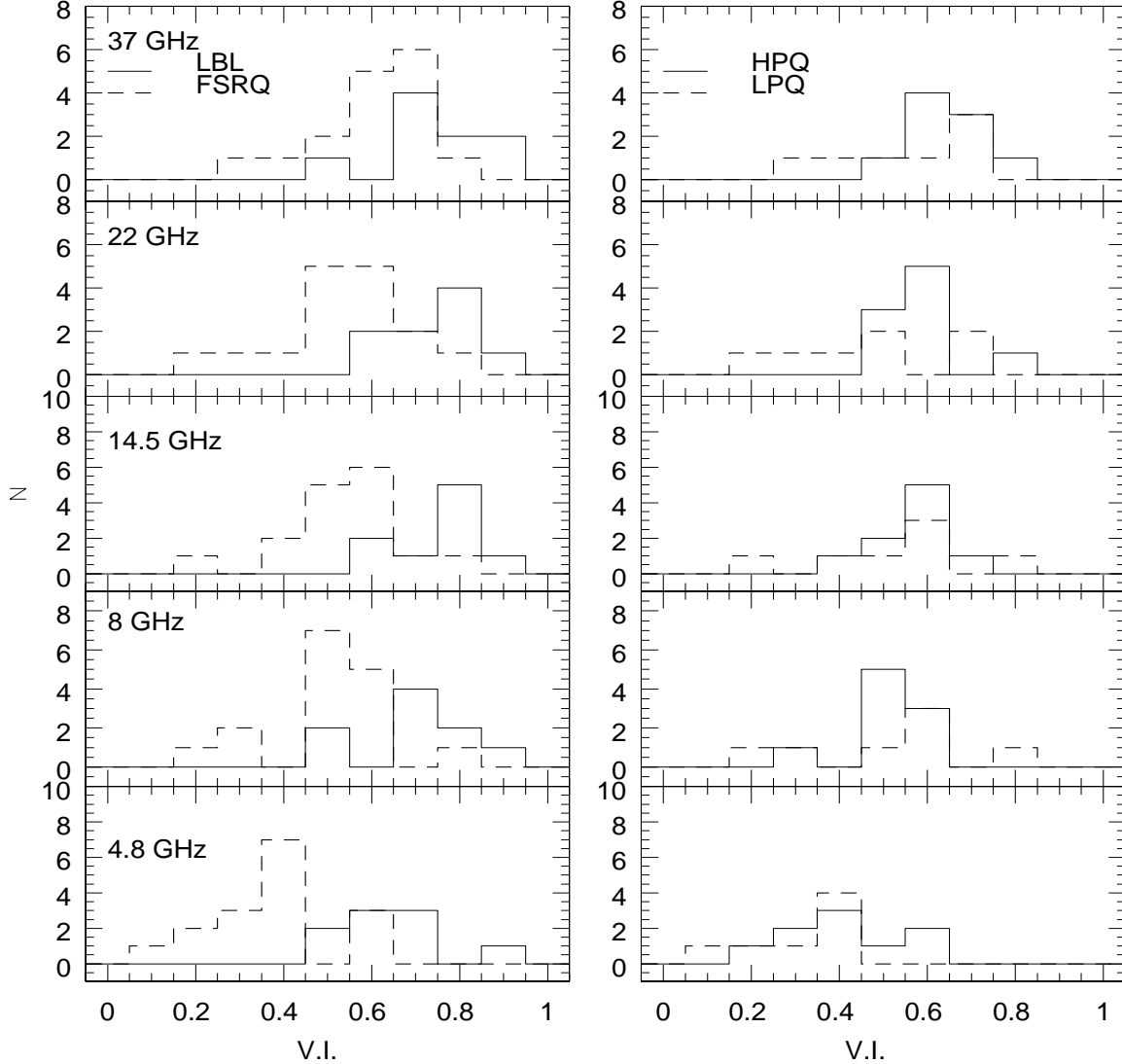
Table 5 gives the mean values of the variability index (V.I.) and their errors at 4.8, 8, 14.5, 22, and 37 GHz for the 25 blazars (9 LBLs and 16 FSRQs) in the U∩M sample. Of the 16 FSRQs, 9 are HPQs and 7 are LPQs; we have

also computed the V.I. for each of these sub-classes. At all frequencies we get systematically higher V.I.s for LBLs than for FSRQs (see also Fig. 7), consistent with the results by Aller et al. (1999). The Kolmogorov-Smirnov (KS) test shows that the differences among the two populations are significant: the probability that the two distributions come from the same parent population is $\simeq 3.1 \times 10^{-3}$, $\simeq 2.4 \times 10^{-3}$, $\simeq 4.2 \times 10^{-3}$, $\simeq 8.6 \times 10^{-3}$, and 9.1×10^{-5} , at 37, 22, 14.5, 8, and 4.8 GHz respectively (see Table 6).

The mean V.I. of FSRQ is higher at higher frequencies: it is $\simeq 0.38$ at 4.8 GHz and becomes $\simeq 0.61$ at 37 GHz. Again, the KS test confirm that the effect is statistically significant: the probability that the distributions at 4.8 and 37 GHz come from the same parent population is $\simeq 4.9 \times 10^{-5}$. The frequency dependence is less clear in the case of LBLs, which have large V.I.s at all frequencies. Still, their mean V.I. increases from $\simeq 0.59$ at 4.8 GHz to $\simeq 0.74$ at 37 GHz; the significance of the difference between the distributions at the two frequencies is $\simeq 4.4 \times 10^{-3}$. The frequency dependence of the V.I. is consistent with the notion that, at lower and lower frequencies, an increasing fraction of the observed emission is produced on larger and larger scales and is therefore less variable on the timescales covered by monitoring programs. At all frequencies the mean V.I. of High-Polarization Quasars (HPQs) is slightly higher than that of Low-Polarization Quasars (LPQs); the difference, however, has always a low statistical significance.

Table 8. Mean values of the log of the structure function timescales.

Type	37 GHz	22 GHz	14.5 GHz	8 GHz	4.8 GHz
all	0.04 ± 0.07	0.10 ± 0.08	0.26 ± 0.09	0.27 ± 0.09	0.40 ± 0.10
LBL	-0.03 ± 0.07	0.20 ± 0.16	0.20 ± 0.13	0.04 ± 0.12	0.29 ± 0.16
FSRQ	0.09 ± 0.10	0.07 ± 0.10	0.33 ± 0.11	0.41 ± 0.13	0.46 ± 0.13
HPQ	0.06 ± 0.13	0.05 ± 0.13	0.13 ± 0.10	0.08 ± 0.12	0.19 ± 0.14
LPQ	0.17 ± 0.17	0.13 ± 0.15	0.46 ± 0.22	0.61 ± 0.26	0.64 ± 0.26

**Fig. 7.** Variability index distributions at different frequencies for the $U \cap M$ sample.

4.2. Structure function

Another useful method for quantitatively investigating variability properties is the so called structure function (S.F.) analysis (Simonetti et al. 1985; Hughes et al. 1992). We have computed the quantities commonly used to characterize the first order S.F., defined as $D(\tau) = \langle [S(t) - S(t+\tau)]^2 \rangle$, namely its slope ($d \log D / d \log \tau$) and the time-

scale, i.e. the time lag of the turnover of the S.F., which may measure the minimum time scale of uncorrelated behavior or, in the case of flicker noise, the minimum time scale in the distribution of response times (Hughes et al. 1992).

In Fig. 8 we show the structure functions at 22 GHz for the 4 sources for which we have the best evidence of periodicity. The value of the derived period is indicated by the

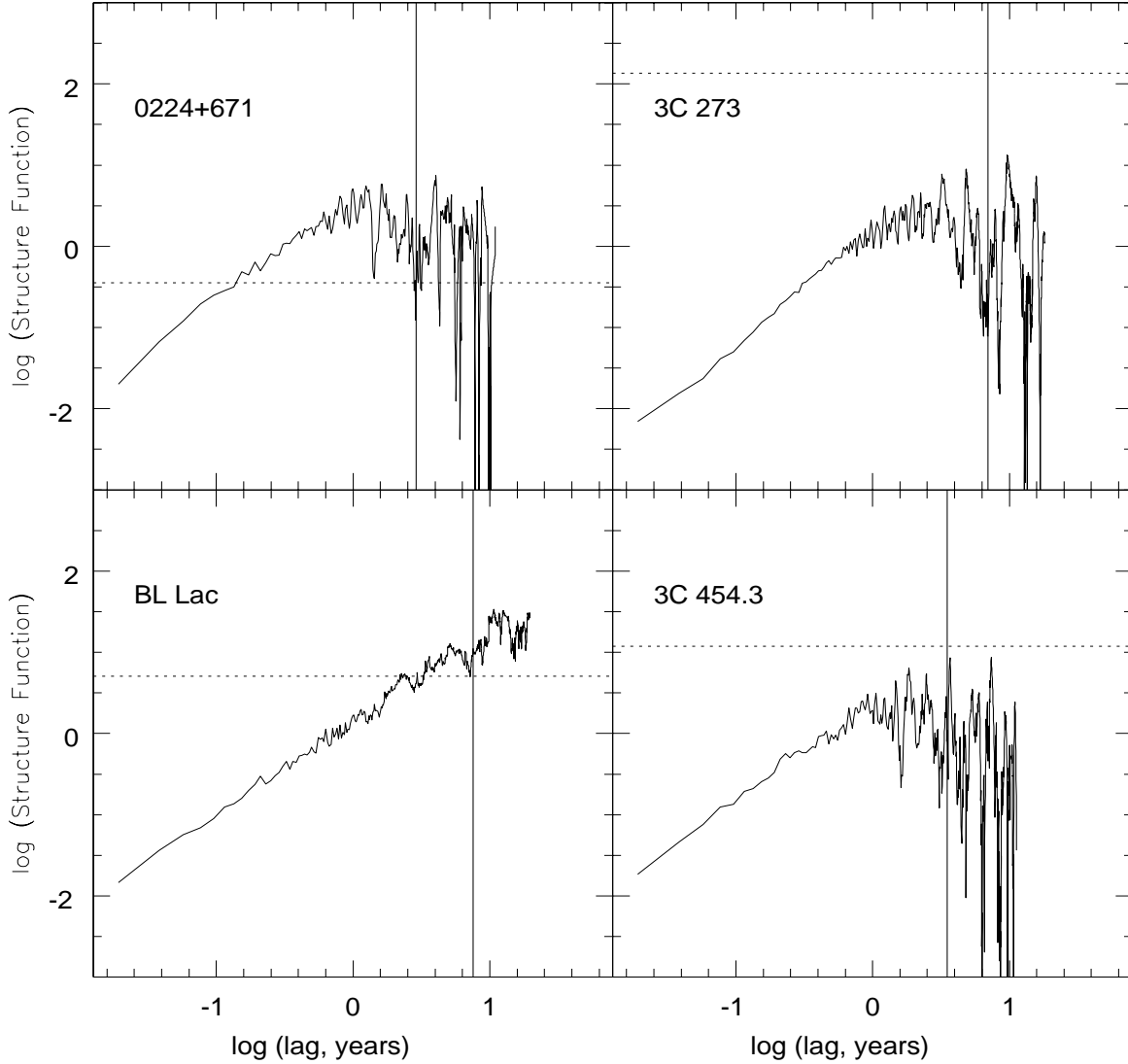


Fig. 8. Structure functions at 22 GHz of the 4 sources for which we have the best evidences of periodicity. The values of the periods are indicated by the vertical lines, while the dotted horizontal lines show the variance of the process.

vertical line, while the dotted horizontal line corresponds to the variance of the process.

The distributions of slopes and of time-scales (in the source frame) are shown in Figs. 9 and 10, respectively. Panels corresponding to frequencies of up to 14.5 GHz refer to the 39 sources in the U sample, those at higher frequencies to the 25 sources in the U∩M sample. Mean values and dispersions are given in Tables 7 and 8. Slopes and time-scales (or lower limits) could be determined for essentially all sources. The exceptions (sources with very irregular S.F.) are just one at 14.5 and 8 GHz, and 3 at 4.8 GHz. For the sources (2 at 37 and 22 GHz, 10 at 14.5 GHz, 11 at 8 and 4.8 GHz) not showing a plateau we adopted the time base of the data as a lower limit to the time-scale. We further have a small number of sources with a plateau

(1 at 37 GHz, 4 at 14.5 GHz, 1 at 8 GHz, and 2 at 4.8 GHz) or a change of slope (1 at 37 GHz, 2 at 22 GHz, 5 at 14.5 GHz, and 4 at 8 and at 4.8 GHz) at intermediate time lag, which may signal the transition between two different processes; in these cases we have adopted the longer time-scale. For sources with a change of slope we have chosen the steeper value.

The average time-scale tend to be somewhat longer (although the statistical significance of the difference between 37 and 4.8 GHz is, for the full sample, only 1.2×10^{-2}), and the fraction of sources with time-scale exceeding the data time span is larger at lower frequencies. The indication, reported by Hughes et al. (1992), that LBLs have, on average, shorter timescales than FSRQs is not statistically significant in the source frames (see Table 8).

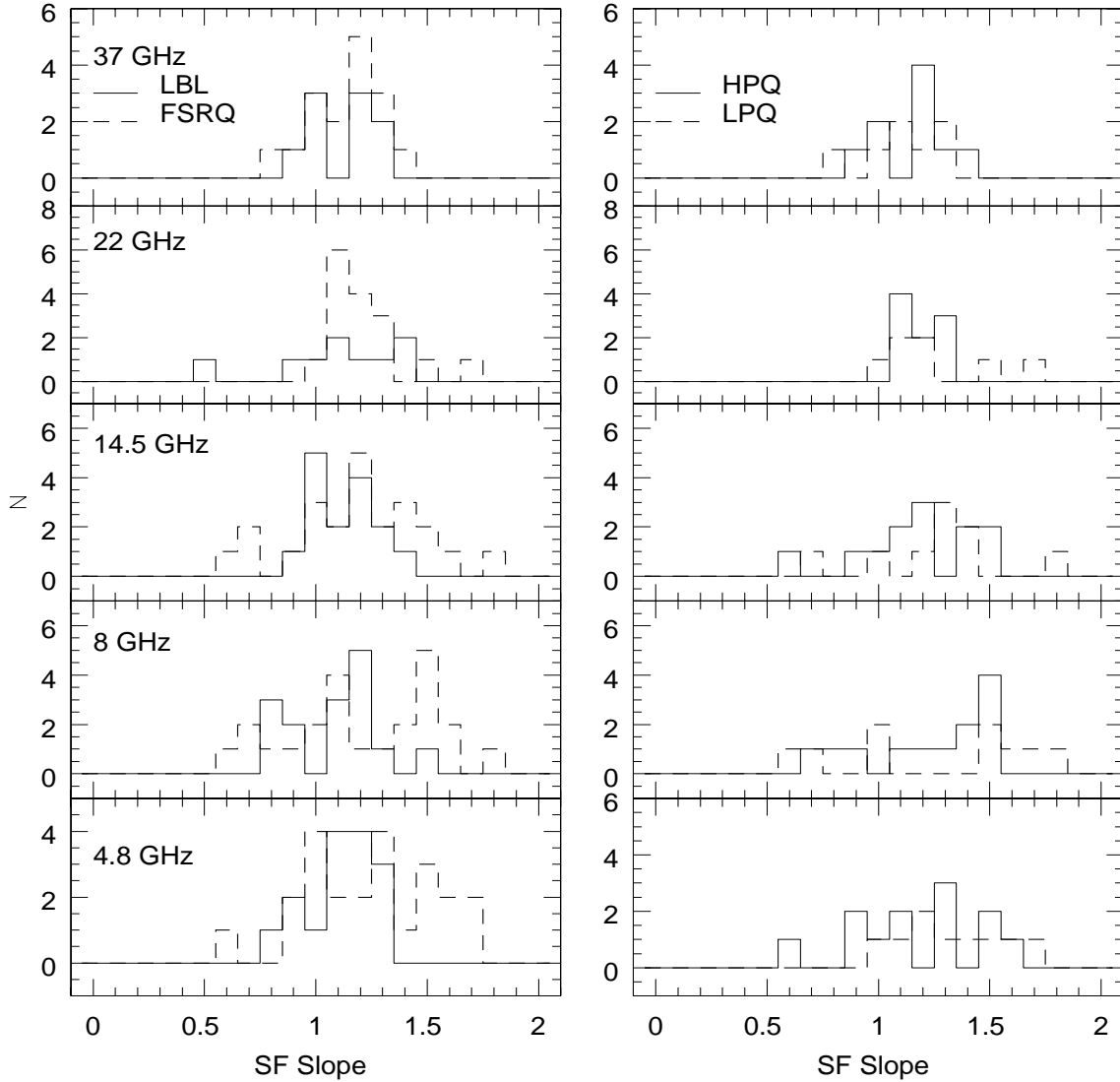


Fig. 9. Distributions of structure function slopes at different frequencies. The results at frequencies ≤ 14.5 GHz refer to the full U sample, while at higher frequencies we are forcefully limited to the 25 sources also monitored at Metsähovi (U \cap M sample).

There is a marginal indication (significance of 2.4×10^{-2} based on the KS test at 8 GHz) of longer timescales for LPQs, compared to HPQs.

No statistically significant variations with frequency of the slope distribution are detected. A visual inspection of Fig. 9 indicates that FSRQs tend to have steeper slopes than LBLs. The average slope of LBLs is $\simeq 1$, the value corresponding to shot noise. In the case of FSRQs, the distributions are somewhat broader and extend to values ≥ 1.5 , particularly at lower frequencies, consistent with the previous findings by Hughes et al. (1992). The KS test yields a probability of 1.2×10^{-2} at 4.8 GHz and of 4.3×10^{-2} at 8 GHz that the distributions for the two populations come from the same parent distribution. No

statistically significant differences are found at higher frequencies. The distributions of LPQs and HPQs are consistent with the same parent population at all frequencies

Possible hints of a correlation of time-scales with slopes were noted by Hughes et al. (1992). A Pearson's test however does not detect any significant correlation among these quantities either for the entire sample or for any sub-population.

4.3. Distribution of intensity variations

As shown by Fig. 11, the distribution of $\log(S/\bar{S})$, where S is the instantaneous flux density at a given frequency and

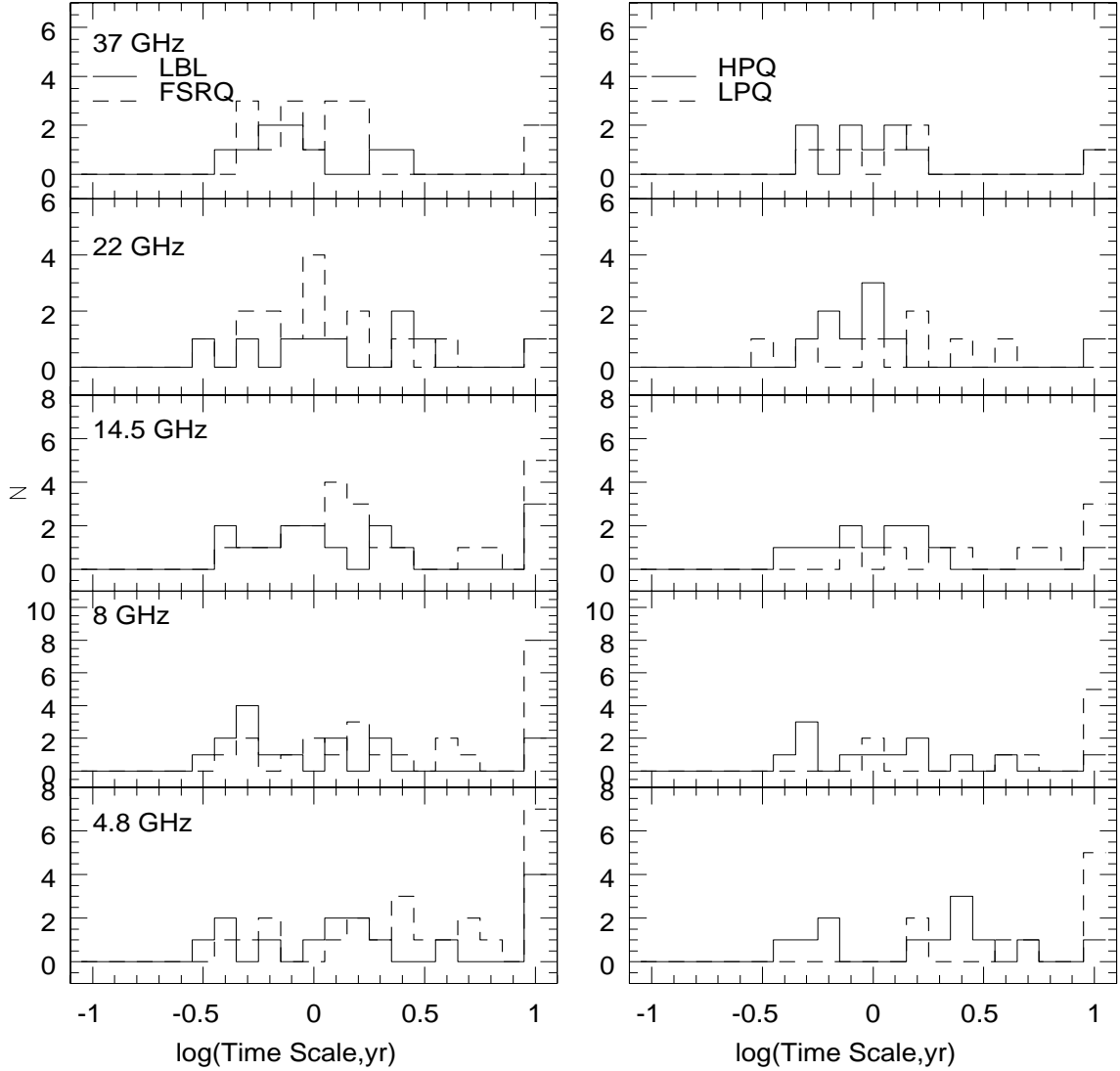


Fig. 10. Distributions of structure function timescales at different frequencies. The samples used are the same as in Fig. 9.

\bar{S} is its average value, broadens with increasing frequency, consistent with the notion that the variability amplitude increases with frequency (Impey & Neugebauer 1988). The frequency dependence of the variance, σ^2 , of the distribution is approximately linear. A fit, shown as a dotted line in the upper part of the panel on the lower right-hand corner of Fig. 11, is given by:

$$\sigma^2 \simeq 1.846 \times 10^{-4} \nu_{\text{GHz}} + 0.01837. \quad (8)$$

The shape of the distribution also changes somewhat with frequency. At high frequencies (22 and 37 GHz), the distribution of intensity fluctuations approaches a log-normal distribution, while at lower frequencies, the distribution of $\log(S/\bar{S})$ is better described by a Laplace or by a Cauchy distribution. The frequency dependencies of the skewness

and of the kurtosis are shown in the middle and on the bottom part of the panel on the lower right-hand corner of Fig. 11.

Variability enhances the bright portion of the luminosity function and of source counts. We have estimated its effect on the 37 and 100 GHz counts of FSRQs and of BL Lacs by convolving the epoch-dependent luminosity functions given by Maraschi & Rovetti (1994) and Urry & Padovani (1995), respectively, with the distribution function of intensity fluctuation shown in the corresponding panel of Fig. 11 at 37 GHz, and with a Gaussian with variance given by Eq. (8) at 100 GHz. As illustrated by Fig. 12, the enhancement of the counts is of about 20–30% at the brightest flux densities. It is thus very likely that a substantial fraction of blazars picked up by the

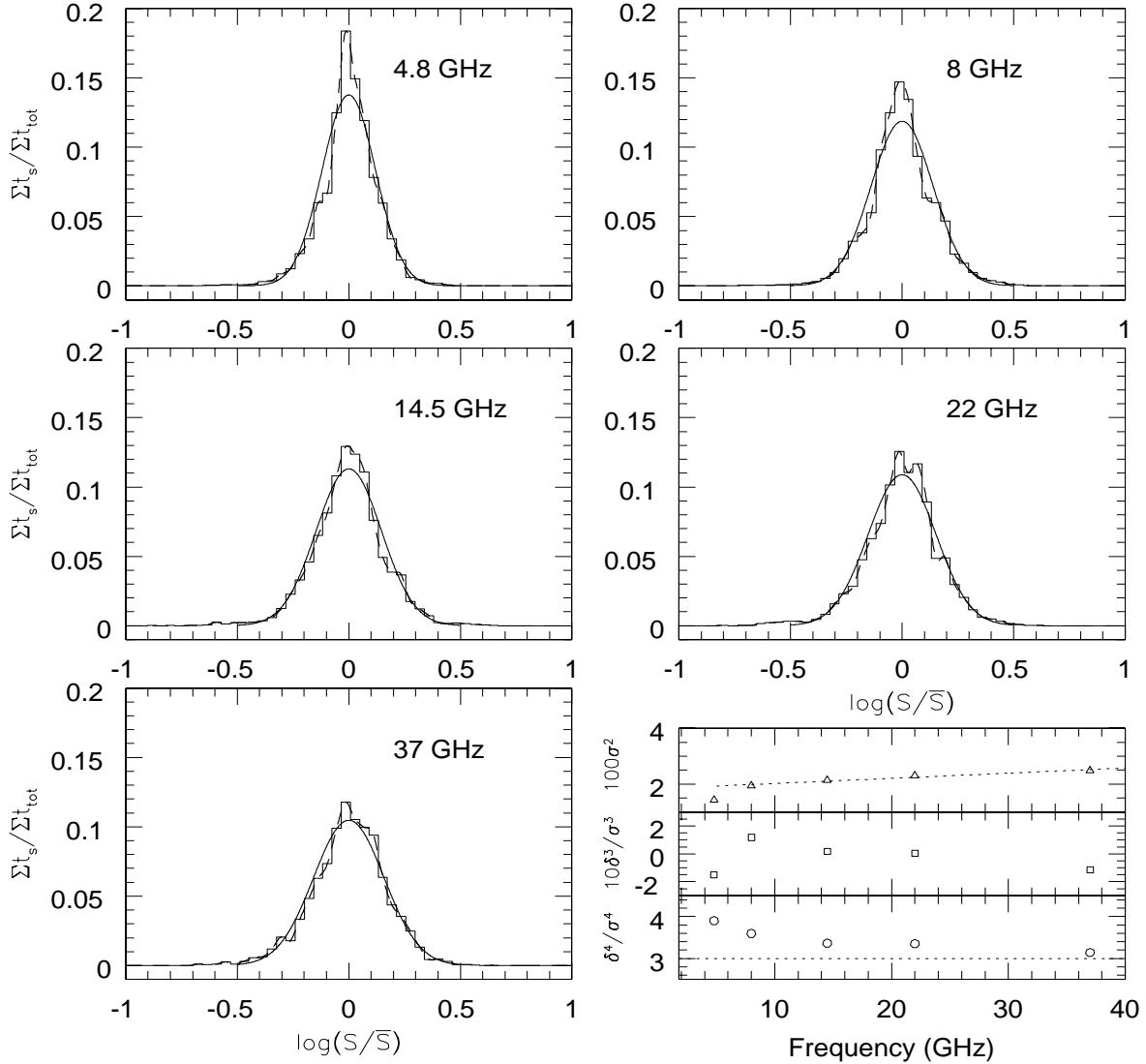


Fig. 11. Probability distribution functions of $\log(S/\bar{S})$ at different frequencies and their Gaussian fits. The panel in the lower right-hand corner shows, as a function of frequency, the variance (multiplied by 100), the skewness ($\times 10$), and the kurtosis.

high-frequency, shallow surveys carried out by the WMAP (Bennett et al. 2003) and PLANCK satellites¹ are in a flaring stage.

5. Discussion and conclusions

Combining the long-term monitoring databases of the University of Michigan Radio Astronomy Observatory (UMRAO) and of the Metsähovi Radio Observatory it is possible to investigate the radio variability properties of a rather rich sample of FSRQs and LBLs over about a decade in frequency.

Our approach has followed different lines of investigation. First, we have addressed the still controversial issue of the existence of periodicities in the radio light curves. In addition to the well known Periodogram method, modified to take into account the effect of uneven sampling, we have applied a more effective technique, never used before in this context, based on the analysis of the signal auto-correlation matrix. We have analyzed the Metsähovi light curves looking for periods shorter than 50% of the maximum admissible period (to avoid aliasing) and detectable (with the same value within the errors) at both 22 and 37 GHz. We have found evidences, confirmed by both techniques, for periodicities in the light curves of 5 (0224+671, 0945 + 408 1226 + 023, 2200 + 420, and 2251 + 158) out

¹ astro.estec.esa.nl/SA-general/Projects/Planck/

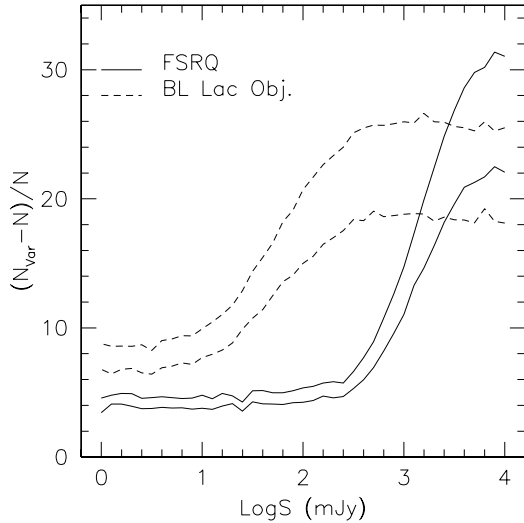


Fig. 12. Effects of variability on counts of FSRQs (solid lines) and of LBLs (dashed lines). For each population, the upper curve refers to 37 GHz, the lower one to 100 GHz. We have adopted a Gaussian distribution for $\log(S/\bar{S})$ with variance given by Eq. (8). Shown are the percentage differences between the counts estimated allowing for variability and those assuming that each source keeps at its average flux \bar{S} .

of the 77 Metsähovi sources having sufficient time coverage for a meaningful analysis to be carried out. For the last three of these sources, consistent periods are found also at the three UMRAO frequencies, while in the case of 0224 + 671 and 0945 + 408 (which were monitored for a relatively short time at Metsähovi) UMRAO data give hints of ill-defined periods a factor of 2 larger than at the Metsähovi frequencies.

The Lomb periodogram method allows us to test quantitatively the significance of the detected periodicities. As shown by Scargle (1982), the false-alarm probability, i.e. the probability that, if we scan M independent frequencies, none has spectral power normalized to the variance of the data larger than z , under the null hypothesis that the data are independent random Gaussian values, is:

$$P(> z) = 1 - (1 - e^{-z})^M. \quad (9)$$

An accurate evaluation of $P(> z)$ is complicated by the difficulty of estimating M (Press et al. 1996, p. 570). However, for any reasonable choice of M , $P(> z)$ turns out to be extremely small (and therefore the significance of the peak in the power spectrum corresponding to the detected period is very high) for 1226 + 023, 2200 + 420, and 2251 + 158 (z amounts to several tens at all frequencies). On the other hand, the false alarms probability may be quite significant for 0224 + 671 and 0945 + 408. As a further test, we have applied the Kolmogorov-Smirnov test to examine the consistency of the data distribution with a

Gaussian random process. This possibility is ruled out for 1226 + 023 and 2251 + 158, but not for the other sources.

We have also investigated the variability index, the structure function, and the distribution of intensity variations of the most extensively monitored sources. We considered UMRAO sources classified either as Low-energy peak BL Lacs or Flat-Spectrum Radio Quasars, monitored at 8 GHz for a total of ≥ 3000 days, with gaps not exceeding 200 days, all times being computed *in the source frame*. The sample comprises 39 sources (24 FSRQs and 15 LBLs), 25 of which (9 LBLs and 16 FSRQs) were also extensively monitored by the Metsähovi group. We have found a statistically significant difference in the distribution of the variability index for LBLs compared to FSRQs, in the sense that the former are more variable. This difference may help shedding light on the relationship between the two blazar sub-classes and is consistent with LBLs having a higher ratio of beamed to unbeamed emission than FSRQs (Fan 2003).

For both populations the variability index steadily increases with increasing frequency. The distribution of intensity variations also broadens with increasing frequency, and approaches a log-normal shape at the highest frequencies. Variability enhances by 20–30%, at bright flux densities, the high frequency counts of extragalactic radio-sources, such as those which will be carried out by the WMAP and PLANCK satellites.

Since the sample is not complete, one should worry about possible selection biases. To test this possibility we have extracted from it a sub-sample 80% complete to a flux limit of 1.2 Jy over the three areas $16^h \leq \alpha \leq 20^h$, $53^\circ \leq \delta \leq 75^\circ$; $21^h \leq \alpha \leq 23^h$, $-8^\circ \leq \delta \leq 45^\circ$; $8^h \leq \alpha \leq 14^h$, $30^\circ \leq \delta \leq 45^\circ$. Such sub-sample comprises only 16 objects (6 LBLs and 10 FSRQs) and is thus too small for our purposes. On the other hand, we did not detect significant differences in the mean properties of sources in the sample of 39 compared to those in the almost complete sub-sample. Also the trends with frequency and the differences among sub-populations are still present. We are therefore confident that, although the sample is not complete, it is essentially unbiased.

Acknowledgements. This research was partly supported by the Italian Space Agency (ASI) and by the Italian MIUR through a COFIN grant. The research by H.D. Aller and M.F. Aller has been supported in part by a series of NSF grants, including AST-9900723. The operation of UMRAO is supported by funds from the University of Michigan Department of Astronomy. We are grateful to the referee, Dr. J.H. Fan, for helpful comments.

References

- Aller, H.D., Aller, M.F., & Hughes, P.A. 1985, ApJ, 298, 296
 Aller, M.F., Aller, H.D., & Hughes, P.A. 1996, in ASP Conf. Ser. 110, Blazar Continuum Variability, eds. H.R. Miller, J.R. Webb, & J.C. Noble, 193

- Aller, M.F., Aller, H.D., & Hughes, P.A. 2003, *ApJ*, 586, 33
- Aller, M.F., Aller, H.D., Hughes, P.A., & Latimer, G.E. 1992, in *Variability of Blazars*, eds. E. Valtaoja & M. Valtonen, Cambridge Univ. Press, p. 126
- Aller, M.F., Aller, H.D., Hughes, P.A. & Latimer, G.E. 1999, *ApJ*, 512, 601
- Aller, H.D., Aller, M.F., Latimer, G.E., & Hodge, P.E. 1985, *ApJS*, 59, 513
- Begelman, M.C., Blandford, R.D., & Rees, M.J. 1980, *Nature*, 287, 307
- Bennett, C., Hill, R.S., Hinshaw, G., et al. 2003, *ApJ*, submitted, astro-ph/0302208
- Bondi, M., Padrielli, L., Fanti, R., et al. 1996, *A&AS*, 120, 89
- Camenzind, M., & Krockenberger, M. 1992, *A&A*, 255, 59
- Deeming, T. J. 1975, *Ap&SS* 36, 137
- Donato, D., Ghisellini, G., Tagliaferri, G., & Fossati, G. 2001, *A&A*, 375, 739
- Fan, J. 2000, in *Proc. Pacific Rim Conference, Stellar Astrophysics*, eds. L.S. Cheng, H.F. Chau, K.L. Chan, & K.C. Leung, Kluwer Academic Pub., The Netherlands, 319
- Fan, J.H. 2003, *ApJ*, 585, L23
- Fan, J.H., Lin, R.G., Xie, G.Z., et al. 2002, *A&A*, 381, 1
- Fernie, J.D. 1979, *PASP*, 91, 67
- Ghisellini, G., Padovani, P., Celotti, A., & Maraschi, L. 1993, *ApJ*, 407, 65
- Hagen-Thorn, V.A., Marchenko, S.G., Mikolaichuk, O.V., & Yakovleva, V.A. 1997, *ARep*, 41, 154
- Horowitz, L.L. 1974, *IEEE Trans.*, ASSP-22, 22
- Horne, J.H. & Baliunas, S.L. 1986, *ApJ*, 302, 757
- Hughes, P.A., Aller, H.D., & Aller, M.F. 1992, *ApJ*, 396, 469
- Hughes, P.A., Aller, H.D., & Aller, M.F. 1998, *ApJ*, 503, 662
- Impey, C.D., & Neugebauer, G. 1988, *AJ*, 95, 307
- Kay, S.M. 1988, *Modern spectral estimation: theory and application*, Prentice-Hall Englewood Cliffs, N.Y.
- Karhunen, J., & Joutsensalo, J. 1994, *Neural Networks* 7, 113
- Karhunen, J., & Joutsensalo, J. 1995, *Neural Networks*, 8, 549
- Kelly, B.C., Hughes, P.A., Aller, H.D., & Aller, M.F. 2003, *ApJ*, 591, 695
- Kovalev, Y.Y., Kovalev, Y.A., Nizhelsky, N.A., & Bogdantsov, A.B. 2002, *PASA*, 19, 83
- Kühr, H., Witzel, A., Pauliny-Toth, I.I.K., & Nauber, U. 1981, *A&AS*, 45, 367
- Lainela, M., & Valtaoja, E. 1993, *ApJ*, 416, 485
- Lähteenmäki, A., & Valtaoja, E. 1999, *ApJ*, 521, 493
- Lähteenmäki, A., Valtaoja, E., & Wiik, K. 1999, *ApJ*, 511, 112
- Lainela, M., Takalo, L.O., Sillanpää, A., et al. 1999, *ApJ*, 521, 561
- Lomb, N.R., 1976, *Ap&SS* 39, 447
- Maraschi, L., & Rovetti, F. 1994, *ApJ*, 436, 79
- Marchenko, S.G., et al. 1996, *proc. int. workshop "Blazar continuum variability"*, ed. H.R. Miller, J.R. Webb, & J.C. Noble, ASP Conf. Ser. 110, p. 105
- Marscher, A.P., & Gear, W.K. 1985, *ApJ*, 298, 114
- Marple, S.L. 1987, *Digital Spectral analysis with applications*, Prentice Hall: Englewood Cliffs, N.Y.
- Marscher, A.P. 1996, in *ASP Conf. Ser.110, Blazar Continuum Variability*, eds. H.R. Miller, J.R. Webb, & J.C. Noble, 248
- Oppenheim, A. V., & Schaffer, R. W. 1965, *Digital signal processing*
- Padovani, P., & Giommi, P. 1995, *ApJ*, 444, 567
- Pietilä, H., Takalo, L.O., Tosti, G., et al. 1999, *A&A*, 345, 760
- Press, W.H., Teukolski, S.A., Vetterling, W.T., & Flannery, B.P. 1996, *Numerical Recipes in C: The Art of Scientific Computing*, Cambridge University Press, Cambridge
- Raiteri, C.M., Villata, M., Tosti, G., et al. 2003, astro-ph/0302518
- Raiteri, C.M., Villata, M., Aller, H.D., et al. 2001, *A&A*, 337, 396
- Roy, M., Papadakis, I.E., Ramos-Colón, E., Sambruna, R., et al. 2000, *ApJ*, 545, 758
- Scargle, J.D. 1982, *ApJ* 263, 835
- Sillanpää, A., Haarala, S., Valtonen, M.J., Sundelius, B., & Byrd, G.G. 1988, *ApJ*, 325, 628
- Sillanpää, A., Takalo, L.O., Pursimo, T., et al. 1996, *A&A*, 305, L17
- Simonetti, J.H., Cordes, J.M., & Heeschen, D.S. 1985, *ApJ*, 296, 46
- Stickel, M., Meisenheimer, K., & Kühr, H. 1994, *A&AS*, 105, 211
- Tagliaferri, R., Ciaramella, A., Milano, L., Barone, F., & Longo, G. 1999, *A & AS*, 137, 391
- Teräsrananta, H., Tornikoski, M., Mujunen, A., et al. 1998, *A&AS*, 91, 121
- Teräsrananta, H., & Valtaoja, E. 1994, *A&A*, 283, 51
- Ulrich, M.-H., Maraschi, L., & Urry, C.M. 1997, *ARA&A*, 35, 445
- Urry, C.M. 1999, *APh*, 11, 159
- Urry, C.M., & Padovani, P. 1995, *PASP*, 107, 803
- Valtaoja, E., Lähteenmäki, A., Teräsrananta H., & Lainela, M. 1999, *ApJS*, 120, 95